Northumbria Research Link

Citation: Trinh, Luan, Vo, Thuc, Thai, Huu-Tai and Nguyen, Trung-Kien (2016) An analytical method for the vibration and buckling of functionally graded beams under mechanical and thermal loads. Composites Part B: Engineering, 100. pp. 152-163. ISSN 1359-8368

Published by: Elsevier

URL: http://dx.doi.org/10.1016/j.compositesb.2016.06.06... <http://dx.doi.org/10.1016/j.compositesb.2016.06.067>

This version was downloaded from Northumbria Research Link: http://nrl.northumbria.ac.uk/27858/

Northumbria University has developed Northumbria Research Link (NRL) to enable users to access the University's research output. Copyright © and moral rights for items on NRL are retained by the individual author(s) and/or other copyright owners. Single copies of full items can be reproduced, displayed or performed, and given to third parties in any format or medium for personal research or study, educational, or not-for-profit purposes without prior permission or charge, provided the authors, title and full bibliographic details are given, as well as a hyperlink and/or URL to the original metadata page. The content must not be changed in any way. Full items must not be sold commercially in any format or medium without formal permission of the copyright holder. The full policy is available online: http://nrl.northumbria.ac.uk/policies.html

This document may differ from the final, published version of the research and has been made available online in accordance with publisher policies. To read and/or cite from the published version of the research, please visit the publisher's website (a subscription may be required.)

www.northumbria.ac.uk/nrl

northumbria UNIVERSITY NEWCASTLE

An analytical method for the vibration and buckling of functionally graded beams under mechanical and thermal loads

Luan C. Trinh [a,c], Thuc P. Vo [a,*], Huu-Tai Thai[b], Trung-Kien Nguyen[c]

[a] Department of Mechanical and Construction Engineering, Northumbria University, Ellison Place, Newcastle upon Tyne NE1 8ST, UK

[b] School of Engineering and Mathematical Sciences, La Trobe University, Bundoora, VIC 3086, Australia

[c] Faculty of Civil Engineering and Applied Mechanics, University of Technical Education Ho Chi Minh City, 1 Vo Van Ngan Street, Thu Duc District, Ho Chi Minh City, Vietnam.

Abstract

An analytical method for vibration and buckling behaviours of Functionally Graded (FG) beams with various boundary conditions under mechanical and thermal loads is presented. Based on linear strain-displacement relations, equations of motion and essential boundary conditions are derived from Hamilton's principle. In order to account for thermal effects, three cases of the temperature rise through the thickness, which are uniform, linear and nonlinear, are considered. The exact solutions are derived using the state space approach. Numerical results are presented to investigate the effects of boundary conditions, temperature distributions, material parameters and slenderness ratios on the critical temperatures, critical buckling loads, and natural frequencies as well as load-frequencies curves, temperature-frequencies curves of FG beams under thermal/mechanical loads. The accuracy and effectiveness of proposed model are verified by comparison with previous research.

Keywords: buckling, vibration, functionally graded beam, state space approach.

* Corresponding author. Tel.: +44 (0) 191 243 7856

E-mail address: luanc.trinh@gmail.com (Luan C. Trinh); thuc.vo@northumbria.ac.uk (Thuc P. Vo).

1. Introduction

Functionally graded materials (FGMs) are a class of composites materials in which the material properties gradually vary in a specific direction. By this way, the distribution of strength and stiffness can be customised in a designable manner and the delamination which may occur in laminated composites can be avoided. Due to the excellent properties in mechanical and thermal behaviours, a wide range of application for functionally graded (FG) structures can be found in different fields, leading to the intensive study in many types of FG structures in the last three decades.

By using various theories such as The Classical Beam Theory (CBT), First-order Beam Theory (FOBT), Higher-order Beam Theory (HOBT), Quasi-3D beam theory and Carrera Unified Formulation (CUF), many numerical methods have been developed to deal with vibration and buckling behaviours of FG beams under mechanical/thermal loads. Some of popular numerical approaches are Lagrange multipliers, Rayleigh Ritz method, dynamic stiffness formulation, Chebyshev collocation method, finite element method and differential quadrature method [1-15]. For analytical approaches, a Navier solution has been widely used to study various mechanical behaviours of simply supported beams [16-20]. In addition, another analytical solution based on the state space approach, which can deal with different boundary conditions, was proposed by Khdeir and Reddy [21-23] to study the behaviour of cross-ply laminated beams. This approach was also applied for the vibration analysis of FG and FG sandwich beams [24, 25]. Regarding the thermal environment, FG beams can be designed in a smart way to adapt the environment changes, which results in a good attention in studying such behaviours. Sankar and Tzeng [26] used CBT to study the thermal stresses of simply supported FG beams. The FOBT was employed to investigate various behaviours of FG beams such as dynamic responses under a moving load [27], thermal stability with non-linear hardening elastic foundations [28], thermal dynamic buckling [29], and thermal buckling and post-buckling with non-linear elastic foundation [30]. Wattanasakulpong et al. [31] used Ritz method based on the HOBT to study the buckling and vibration of FG beams, however, it was limit

on uniform temperature distribution only. Based on CUF, Giunta et al. [32] developed Navier solution to analyse the static behaviour of FG beams under thermo-mechanical loads. However, as far as the authors are aware, there is no analytical solution for vibration and buckling of FG beams using HOBT with various boundary conditions under mechanical/thermal loads in a unitary manner. In addition, effects of various temperature distributions on natural frequencies and critical temperatures of FG beams are also need further studies. As a result, it is also the main objective of this paper. Based on linear strain-displacement relations, equations of motion and the essential boundary conditions are derived from Hamilton's principle. State space-based analytical approach is used to obtain closed-form solutions for FG beams with various configurations. Three cases of the temperature rise through the thickness, which are uniform, linear and nonlinear, are considered. Numerical results are presented for FG beams with various boundary conditions, temperature distributions and slenderness ratios to investigate the critical temperatures/loads, and natural frequencies as well as load-frequencies curves, temperature-frequencies curves. The accuracy and effectiveness of proposed model are verified by comparison with previous research.

2. Theoretical formulation

2.1. Functionally graded beams and temperature-dependent material properties

Consider a FG beam made from metal and ceramic with the span of a and rectangular cross-section of $b \times h$, as shown in Fig.1. Volume fraction of ceramic is given by power law distribution:

$$V_c\left(z\right) = \left(\frac{z}{h} + \frac{1}{2}\right)^p \tag{1}$$

where p is the material parameter.

The thermo-elastic material properties are considered as a function of temperature T and can be calculated for ceramic and metal as described in [33]:

$$P\left(T\right) = P_0\left(P_{-1}T^{-1} + 1 + P_1T + P_2T^2 + P_3T^3\right) \tag{2}$$

where P denotes Young's modulus E, mass density ρ and thermal expansion coefficient α, respectively. P_{-1}, P_1, P_2 and P_3 are the temperature dependent coefficients, which are listed in Table 1 for various materials. Fig. 2 presents the material properties of ceramics and metals with respect to the temperature change. Based on the power rule together with the temperature-dependence described in Eq. (2), the typical material properties $P(z,T)$ of beam through the thickness are described as:

$$P(z,T) = \left[P_c(T) \quad P_m(T)\right] V_c(z) \quad P_m(T) \tag{3}$$

The material properties are calculated by Eq. (2) for ceramic and metal at the specific temperature and followed by Eq. (3) to obtain the values at z. It should be noticed that the Poisson's ratio υ is evaluated as the average of ceramic and metal values at $T_0 = 300K$.

2.2. Temperature distribution

2.2.1. Uniform Temperature Rise (UTR)

The temperature of the whole beam is assumed uniform and increased from $T_0 = 300K$ to the current value. It means that the temperature at a point is $T(z) = T_0 + \Delta T$, where ΔT is the temperature rise.

2.2.2. Linear Temperature Rise (LNR)

The temperature in the ceramic and metal faces of FG beam is assumed to be T_c and T_m. In this case, the temperature on the metal surface is supposed to be $T_m = 305K$, whereas on the ceramic surface it is surged to $T_c = T_0 + \Delta T$. With the assumption of linear distribution, the temperature through the thickness can be determined as:

$$T(z) = T_m + \Delta T\left(\frac{1}{2} + \frac{z}{h}\right) \tag{4}$$

2.2.3. Non-linear Temperature Rise (NLNR)

The applied temperature is similar to the case of LNR; however, the temperature distribution is set to follow the heat conduction rule and obtained by solving the steady state equation [27] as:

$$T(z)=T_m+\frac{T_c-T_m}{C}\left(\begin{array}{l}V_f-\frac{K_{cm}}{(p+1)K_{cm}}V_f^{p+1}+\frac{K_{cm}^2}{(2p+1)K_m^2}V_f^{2p+1}-\frac{K_{cm}^3}{(3p+1)K_m^3}V_f^{3p+1}\\+\frac{K_{cm}^4}{(4p+1)K_m^4}V_f^{4p+1}-\frac{K_{cm}^5}{(5p+1)K_m^5}V_f^{5p+1}\end{array}\right) \quad (5)$$

where $C=1+\frac{K_{cm}}{(p+1)K_{cm}}+\frac{K_{cm}^2}{(2p+1)K_m^2}+\frac{K_{cm}^3}{(3p+1)K_m^3}+\frac{K_{cm}^4}{(4p+1)K_m^4}+\frac{K_{cm}^5}{(5p+1)K_m^5}$; $K_{cm}=K_c-K_m$

and K_c and K_m are the thermal conductivity of ceramic and metal calculated at the surfaces.

2.3. Kinematics

Assuming that the deformation of FG beam is only in the $x-z$ plane and let $u(x,z,t)$ and $w(x,z,t)$ be the axial and transverse displacements at an arbitrary point. These components can be expressed in terms of the displacement components on the neutral line as:

$$u(x,z,t)=U(x,t)-zW'(x,t)+\left(z-\frac{4z^3}{3h^2}\right)\varphi_x(x,t)=U(x,t)-zW'(x,t)+f(z)\varphi_x(x,t) \quad (6a)$$

$$w(x,z,t)=W(x,t) \quad (6b)$$

where $U(x,t)$, $W(x,t)$ and $\varphi_x(x,t)$ denote the displacements along x,z axes and the rotational angle at a point on the neutral line. The prime (‘) expresses the derivatives of the functions in accordance with x coordinate.

Based on the linear strain –displacement relations, the axial and shear strains can be given as:

$$\varepsilon_x=\frac{\partial u}{\partial x}=U'-zW''+f(z)\varphi_x' \quad (7a)$$

$$\gamma_{xz}=\frac{\partial u}{\partial z}+\frac{\partial w}{\partial x}=\left(1-\frac{4z^2}{h^2}\right)\varphi_x=g(z)\varphi_x \quad (7b)$$

where $g(z)=\frac{df}{dz}=\left(1-\frac{4z^2}{h^2}\right)$.

2.4. Variational formulation

The governing equations of motion are obtained based on Hamilton's principle, which is expressed as:

$$\int_{t_1}^{t_2} \left(\delta \mathrm{U} + \delta \mathrm{V} - \delta K\right) dt = 0 \tag{8}$$

where $\delta \mathrm{U}$, $\delta \mathrm{V}$ denote the virtual variation of the strain energy, external work by axial load or thermal expansion and δK is the kinetic energy.

The virtual variation of the strain energy is given by:

$$\delta \mathrm{U} = \int_{-\frac{a}{2}}^{\frac{a}{2}} \int_0^b \int_{-\frac{h}{2}}^{\frac{h}{2}} \left(\sigma_x \delta \varepsilon_x \quad \sigma_{xz} \delta \gamma_{xz}\right) dz dy dx = \int_{-\frac{a}{2}}^{\frac{a}{2}} \left(N_x \delta U^{'} - M_x \delta U^{''} + P_x \delta \varphi_x^{'} + Q_{xz} g(z) \delta \varphi_x\right) dx \tag{9}$$

where the stress resultants N_x, M_x, P_x and Q_{xz} can be defined as:

$$N_x = \int_{-\frac{h}{2}}^{\frac{h}{2}} \sigma_x b dz \tag{10a}$$

$$M_x = \int_{-\frac{h}{2}}^{\frac{h}{2}} \sigma_x b z dz \tag{10b}$$

$$P_x = \int_{-\frac{h}{2}}^{\frac{h}{2}} \sigma_x b f\left(z\right) dz \tag{10c}$$

$$Q_{xz} = \int_{-\frac{h}{2}}^{\frac{h}{2}} \sigma_{xz} b dz \tag{10d}$$

The virtual variation of the external work in linear buckling analysis can be determined as:

$$\delta V = -\int_{-\frac{a}{2}}^{\frac{a}{2}} P_0 W^{'} \delta W^{'} dx \tag{11}$$

Where P_0 is the mechanical load or the thermal stress resultant, which is discussed in next section.

Finally, the virtual variation of the kinetic energy is formed as:

$$\delta K = \int_{-\frac{a}{2}}^{\frac{a}{2}} \left(\dot{u}\delta\dot{u} + \dot{w}\delta\dot{w}\right)\rho(z)b\,dx$$

$$= \int_{-\frac{a}{2}}^{\frac{a}{2}} \begin{pmatrix} I_0\left(\dot{U}\delta\dot{U} + \dot{W}\delta\dot{W}\right) - I_1\left(\dot{W}'\delta\dot{U} + \dot{U}\delta\dot{W}'\right) + I_2\dot{W}'\delta\dot{W}' + I_f\left(\dot{\varphi}_x\delta\dot{U} + \dot{U}\delta\dot{\varphi}_x\right) \\ -I_{fz}\left(\dot{\varphi}_x\delta\dot{W}' + \dot{W}'\delta\dot{\varphi}_x\right) + I_{f^2}\dot{\varphi}_x\delta\dot{\varphi}_x \end{pmatrix} dx \tag{12}$$

where (.) denotes the time derivative, and

$$\left(I_0, I_1, I_2, I_f, I_{fz}, I_{f^2}\right) = \int_{-\frac{h}{2}}^{\frac{h}{2}} \left(1, z, z^2, f, zf, f^2\right)\rho(z)b\,dz \tag{13}$$

2.5. Constitutive equations

The stress-strain relation for elastic FG beams can be written as:

$$\sigma_x = E(z)\left[\varepsilon_x - \alpha(z)\left(T - T_0\right)\right] = Q_{11}\varepsilon_x + \sigma_x^T \tag{14a}$$

$$\sigma_{xz} = = \frac{E}{2(1+\upsilon)}\gamma_{xz} \quad Q_{55}\gamma_{xz} \tag{14b}$$

Where $Q_{11} = E(z)$, $Q_{55} = \dfrac{E(z)}{2(1+\upsilon)}$ and $\sigma_x^T = E(z)\left(T - T_0\right)$.

The stress resultants are described in terms of displacement components by substituting Eq. (7) into Eq. (14) and replacing the outcomes to Eq. (10), as shown in Eq. (15):

$$\begin{Bmatrix} N_x \\ M_x \\ P_x \\ Q_{xz} \end{Bmatrix} = \begin{bmatrix} A & B & B & 0 \\ B & D & F & 0 \\ C & F & H & 0 \\ 0 & 0 & 0 & A_s \end{bmatrix} \begin{Bmatrix} U' \\ -W'' \\ \varphi'_x \\ g(z)\varphi_x \end{Bmatrix} \begin{Bmatrix} N_x^T \\ M_x^T \\ P_x^T \\ Q_x^T \end{Bmatrix} \tag{15}$$

where

$$\left(A, B, D, C, F, H\right) = \int_A Q_{11}\left(1, z, z^2, f, zf, f^2\right)dA \tag{16a}$$

$$A_S = \int_A Q_{55}\,dA \tag{16b}$$

$$\begin{Bmatrix} N_x^T \\ M_x^T \\ P_x^T \\ Q_x^T \end{Bmatrix} = \int_{-\frac{h}{2}}^{\frac{h}{2}} Q_{11}\alpha(z)(T \quad T_0) \begin{Bmatrix} 1 \\ z \\ z^3 \\ 0 \end{Bmatrix} dz \tag{16c}$$

It is noticeable that M_x^T and P_x^T are neglected in this paper.

2.6. Governing equations of motion and the state space solution

By substituting Eqs. (9), (11) and (12) into Eq. (8), integrating the equation by part, and collecting the coefficients of $\delta U, \delta\varphi_x$ and δW , the governing equations of motion are obtained as:

$$N_x^{'} = I_0\ddot{U} - I_1\ddot{W}^{'} + I_f\ddot{\varphi}_x \tag{17a}$$

$$M_x^{''} - P_0W^{''} = I_0\ddot{W} + I_1\ddot{U}^{'} - I_2\ddot{W}^{''} + I_{fz}\ddot{\varphi}_x^{'} \tag{17b}$$

$$P_x^{'} - Q_{xz}g(z) = I_f\ddot{U} - I_{fz}\ddot{W}^{'} + I_{f^2}\ddot{\varphi}_x \tag{17c}$$

By using the state space approach [34], the displacement components can be expressed as:

$$\begin{Bmatrix} U(x,t) \\ \varphi_x(x,t) \\ W(x,t) \end{Bmatrix} = \begin{Bmatrix} U(x) \\ \varphi_x(x) \\ W(x) \end{Bmatrix} e^{i\omega t} \tag{18}$$

where ω is the eigen-frequency.

2.6.1. Vibration analysis

By substituting Eq. (18) into Eq. (17), a system of ordinary differential equations is obtained:

$$U^{''} = a_1U + a_2\varphi_x + a_3W^{'} + a_4W^{'''} \tag{19a}$$

$$\varphi_x^{''} = a_5U + a_6\varphi_x + a_7W^{'} + a_8W^{'''} \tag{19b}$$

$$W^{(iv)} = a_9U^{'} + a_{10}\varphi_x^{'} + a_{11}W + a_{12}W^{''} \tag{19c}$$

where the coefficients a_n are described as:

$$a_1 = \frac{e_1 e_8 - e_3 e_4}{e_2 e_8 - e_4^2}\ ,\ \ a_2 = \frac{e_3 e_8 - e_4 e_7}{e_2 e_8 - e_4^2},\ a_3 = \frac{e_5 e_8 - e_4 e_9}{e_2 e_8 - e_4^2},\ a_4 = \frac{-e_6 e_8 + e_4 e_{10}}{e_2 e_8 - e_4^2},$$

$$a_5 = \frac{e_2 e_3 - e_1 e_4}{e_2 e_8 - e_4^2}\ ,\ \ a_6 = \frac{e_2 e_7 - e_3 e_4}{e_2 e_8 - e_4^2},\ a_7 = \frac{e_2 e_9 - e_4 e_5}{e_2 e_8 - e_4^2},\ a_8 = \frac{-e_2 e_{10} + e_4 e_6}{e_2 e_8 - e_4^2},$$

$$a_9 = \frac{a_1 e_6 + a_5 e_{10} - e_5}{e_{12} - a_4 e_6 - a_8 e_{10}}\ ,\ \ a_{10} = \frac{a_2 e_6 + a_6 e_{10} - e_9}{e_{12} - a_4 e_6 - a_8 e_{10}},\ a_{11} = \frac{e_1}{e_{12} - a_4 e_6 - a_8 e_{10}},\ a_{12} = \frac{a_3 e_6 + a_7 e_{10} + e_{11} + P_0}{e_{12} - a_4 e_6 - a_8 e_{10}},$$

in which

$$e_1 = -I_0\omega^2\ ,\ \ e_2 = A,\ e_3 = -J_1\omega^2\ ,\ e_4 = C\ ,\ e_5 = I_1\omega^2\ ,\ e_6 = -B,$$

$$e_7 = \ \ K_2\omega^2 \quad A_s\ ,\ e_8 = H\ ,\ e_9 = J_2\omega^2\ ,\ e_{10} = -F\ ,\ e_{11} = I_2\omega^2\ ,\ e_{12} = -D,$$

The systems of Eq. (19) can be converted into a matrix form using state space approach as:

$$\mathbf{Z}'(x) = \mathbf{T}\mathbf{Z}(x) \tag{20}$$

where the variables are $\mathbf{Z}(x) = \left\{U, U', \varphi_x, \varphi_x', W, W', W'', W'''\right\}$; and matrix $[\mathbf{T}]$ is defined as:

$$[\mathbf{T}] = \begin{bmatrix} 0 & 1 & 0 & 0 & 0 & 0 & 0 & 0 \\ a_1 & 0 & a_2 & 0 & 0 & a_3 & 0 & a_4 \\ 0 & 0 & 0 & 1 & 0 & 0 & 0 & 0 \\ a_5 & 0 & a_6 & 0 & 0 & a_7 & 0 & a_8 \\ 0 & 0 & 0 & 0 & 0 & 1 & 0 & 0 \\ 0 & 0 & 0 & 0 & 0 & 0 & 1 & 0 \\ 0 & 0 & 0 & 0 & 0 & 0 & 0 & 1 \\ 0 & a_9 & 0 & a_{10} & a_{11} & 0 & a_{12} & 0 \end{bmatrix} \tag{21}$$

A formal solution of Eq. (20) is given by:

$$\mathbf{Z}(x) = e^{\mathbf{T}x}\mathbf{K} \tag{22}$$

where $\{\mathbf{K}\}$ is a constant column vector determined from the boundary conditions at $x = \pm a/2$; and

$\left[e^{\mathbf{T}x}\right]$ is the general matrix solution of Eq. (22) which can be expressed as:

$$\left[e^{\mathbf{T}x}\right]=\left[\mathbf{E}\right]\begin{bmatrix} e^{\lambda_1 x} & & 0 \\ & \ddots & \\ 0 & & e^{\lambda_8 x} \end{bmatrix}\left[\mathbf{E}\right]^{-1} \tag{23}$$

in which $\{\boldsymbol{\lambda}\}$ and $[\mathbf{E}]$ are the eigenvalues and corresponding eigenvectors, respectively, associated with the matrix $[\mathbf{T}]$.

The boundary conditions expressed in terms of displacement variables is

Clamped (C): $U=\varphi_x=W=W^{'}=0$ (24a)

Pinned (P): $U=W=AU^{'}-FW^{''}+H\varphi_x^{'}=BU^{'}-DW^{''}+F\varphi_x^{'}=0$ (24b)

Free (F): $$\begin{aligned} &AU^{'}-BW^{''}+C\varphi_x^{'}=BU^{'}-DW^{''}+F\varphi_x^{'}=AU^{'}-FW^{''}+H\varphi_x^{'} \\ &=BU^{''}-DW^{'''}+F\varphi_x^{''}+I_1\omega^2U+J_2\omega^2\varphi_x-I_2\omega^2W^{'}=0 \end{aligned} \tag{24c}$$

2.6.2. Buckling analysis

Similar to the process carried out in previous section, by neglecting some terms related to time derivatives and frequencies, the system of equations expressed in the state space formulation as:

$$U^{''}=a_2\varphi_x+a_4W^{'''} \tag{25a}$$

$$\varphi^{''}=a_6\varphi_x+a_8W^{'''} \tag{25b}$$

$$W^{(iv)}=a_{10}\varphi_x^{'}+a_{12}W^{''} \tag{25c}$$

where the primary variables are reduced to $\mathbf{Z}(x)=\left\{\varphi_x,\varphi_x^{'},W,W^{'},W^{''},W^{'''}\right\}$. Since Eq. (25a) is a induced equation; matrix T, in this case, is assembled by neglecting the first 2 rows and 2 columns of matrix $[\mathbf{T}]$ in Eq. (21).

In addition, because of the multiplicity in eigenvalues ($\lambda_1=\lambda_2=0$), Jordan canonical form is applied

for the general matrix solution:

$$\left[e^{\mathbf{T}x}\right]=\left[\mathbf{E}\right]\begin{bmatrix}1 & x & 0 & 0 & 0 & 0\\ 0 & 1 & 0 & 0 & 0 & 0\\ 0 & 0 & e^{\lambda_3 x} & 0 & 0 & 0\\ 0 & 0 & 0 & e^{\lambda_4 x} & 0 & 0\\ 0 & 0 & 0 & 0 & e^{\lambda_5 x} & 0\\ 0 & 0 & 0 & 0 & 0 & e^{\lambda_6 x}\end{bmatrix}\left[\mathbf{E}\right]^{-1} \tag{26}$$

The boundary conditions expressed in terms of displacement variables in the buckling problem is:

Clamped (C): $\varphi_x = W = W^{'} = 0$ (27a)

Pinned (P): $\varphi_x = \varphi_x^{'} = W^{''} = 0$ (27b)

Free (F): $\varphi_x^{'} = W^{''} = \left(Ba_2 + Fa_6\right)\varphi_x - P_0 W^{'} + \left(Ba_4 + Fa_8 - D\right)W^{'''} = 0$ (27c)

Substituting Eq. (22) into the appropriate boundary conditions in Eq. (24) or Eq. (27), the homogeneous system of equations is obtained in the form:

$$e^{\mathbf{T}x}\mathbf{K} = 0 \tag{28}$$

The non-trivial solutions for Eq. (28) require the determinant of $\left[e^{\mathbf{T}x}\right]$ being zero, from which the frequency or the buckling temperature can be achieved. Due to the presence of frequency or the temperature in $\left[e^{\mathbf{T}x}\right]$, the trial-error process is needed for the solutions.

3. Numerical Examples and Discussion

3.1. Mechanical loads

This section has the aim of presenting a number of results derived from vibration and buckling analyses performed on Al_2O_3/Fe and Al_2O_3/Al beams under axial load. The ceramic component is Al_2O_3 $\left(E_c = 380GPa, \rho_m \quad 3800kg/m^3\right)$ and the metal is either structural steel $\left(E_m = 210GPa, \rho_m \quad 7800kg/m^3\right)$ or Al $\left(E_m = 70GPa, \rho_m = 2702kg/m^3\right)$. The Poisson's ratio is assumed to be constant and indicated in Tables 2-5. In these tables, the dimensionless natural frequencies and buckling loads are $\overline{\omega} = \omega\dfrac{a^2}{h}\sqrt{\dfrac{\rho_m}{E_m}}$ and $\overline{P} = P\dfrac{12a^2}{E_m h^3}$. The first five natural frequencies, critical buckling loads of Al_2O_3/Fe and Al_2O_3/Al beams with various boundary conditions are

displayed in Tables 2-5. It can be seen that the current solutions are in excellent agreement with previous studies for both vibration ([2], [4], [10], [14]) and buckling problems ([10], [33]). It is clear that the critical buckling loads are calculated directly in section 2.6.2. However, they can also be determined by increasing the axial force until the lowest natural frequency vanishes. By using this way, load-frequency curves can be plotted and used to explain the duality between the buckling load and natural frequency. The first load-frequencies with various material parameters and the first five load – frequency curves with $p = 0.5$ of *C*-*C* Al_2O_3/Al beams are plotted in Figs. 3 and 4. It can be seen that the increase of p leads to the reduction of frequencies in any axial load values. As expected, the bending natural frequencies decrease as the axial force changes from tension to compression, while the axial modes (mode 3 for $a/h = 5$ and mode 5 for $a/h = 20$) are almost constant. It is from load-frequency curves that for $(a/h = 5, p = 0.5)$ (Fig. 4), the first, second, third and fourth buckling occurs at $\bar{P}$ = 103.732, 161.925, 237.383 and 274.285, respectively.

3.2 Thermal loads

The following section aims to present the results derived from thermal vibration and buckling analyses of various FG beams including Si_3N_4/SUS304, Al_2O_3/SUS304, ZrO_2/SUS304 and ZrO_2/Ti-6Al-4V. The temperature-dependent properties of these materials are given in Table 1. Three types of temperature distribution through the thickness, which are Uniform Temperature Rise (UTR), Linear Temperature Rise (LNR) and Non-linear Temperature Rise (NLNR), are considered. The temperature distributions and Young's modulus along the thickness direction for Si_3N_4/SUS304 beam at $\Delta T = 0$ and 900K is plotted in Fig. 5.

3.2.1 Uniform Temperature Rise (UTR)

This example aims to verify the accuracy further in thermal vibration and buckling behaviours and to investigate the thermal effect of Temperature Independent (TID) and Temperature Dependence (TD) material properties. The temperature is assumed to be uniform through the thickness. In order to verify with Wattanasakulpong et al. [31], the elastic constants of FG beams in this example are taken as $Q_{11} = \dfrac{E(z)}{1-\upsilon^2}$ and $Q_{55} = \dfrac{E(z)}{2(1+\upsilon)}$; and the thermal stresses are calculated as $\sigma_x^T = -\dfrac{E(z)\alpha(z)\Delta T}{1-\upsilon}$.

The following dimensionless critical temperatures and natural frequencies are used: $\lambda = \Delta T_{cr}\left(\dfrac{a}{h}\right)^2 \alpha_m$ and $\Omega = \omega\dfrac{a^2}{h}\sqrt{\dfrac{I_0}{\int_{-h/2}^{h/2} E(z)\,dz}}$ with α_m being thermal expansion of metals at $T_m = 300(K)$.

Tables 6-8 present the critical temperatures and fundamental frequencies of various FG beams under UTR. The present TID and TD solutions are in good agreement with those from [31] for all boundary conditions and slenderness ratios. These tables also reveal that the TD solution gives significantly lower values compared to TID one, which highlights the importance of temperature dependence in FG beams. Due to this reason, only TD solution is used in the rest of the paper. It can be seen from Table 7 that the difference in buckling behaviour of Si_3N_4 and Al_2O_3 in combination with SUS304 is significant inspite of a slight difference of properties between these two ceramics, whose material properties are shown in Fig. 2. In addition, Ti-6Al-4V presents a much higher buckling temperature over SUS304 in the mixture with the ceramic ZrO_2, especially with a high volume of metal.

The effect of temperature on the fundamental frequencies of various FG beams with $p = 0.2$ and 2 are illustrated in Fig. 6. As the temperature increases, the fundamental frequencies decrease and finally vanish at the critical temperature points. That is also the characteristic of frequency-temperature curves, which can be used to determine the critical temperature of FG beams. For example, with $p = 2$, the critical temperatures of Si_3N_4/SUS304, Al_2O_3/SUS304 and ZrO_2/SUS304 beams are 401.25, 415.14 and 240.65 (K), respectively.

3.2.2 Linear Temperature Rise (LNR) and Nonlinear Temperature Rise (NLNR)

The comparison between UTR and LNR solutions as well as LNR and NLNR solutions for the critical temperatures and natural frequencies of FG beams is given in Tables 9-12. The following dimensionless natural frequency is used: $\bar{\Omega} = \omega a^2 \sqrt{\frac{\rho_c A}{E_c I}}$. The results reported by Ebrahimi and Salari [35] for the case of *P-P* beams using the FOBT are also given for the verification purpose. A good agreement between the present results with previous ones can be observed for various p values. For all boundary conditions and material parameters, the LNR results are significantly greater than those from the UTR. It should be noted that there are some limitations for thermal buckling of moderate thick beams since their critical temperatures are greater than the melting point of the metals, for example with Si_3N_4/SUS304 *C-C* beam $\left(a/h = 20, p = 0\right)$ in Table 9. As expected, the critical temperatures obtained from LNR and NLNR are the same for isotropic beams (Table 12). As p increases, the difference becomes more pronounced with higher values for NLNR solution. Fig. 7 illustrates the critical temperatures of *C-P* FG beams under LNR versus material parameters. It is clear that with the increase of p, the critical temperatures of Si_3N_4/SUS304 and Al_2O_3/SUS304 beams decrease, whereas those of ZrO_2/SUS304 and ZrO_2/Ti-6Al-4V beams increase. Comparing the buckling temperature of ZrO_2/SUS304 and ZrO_2/Ti-6Al-4V beams, values for the latter is lower for

$0 \le p \le 1.2$ but higher for $p > 1.2$ (Fig. 7). A general view of UTR, LNR and NLNR solutions can be seen in Fig. 8. The difference of UTR solution and the others are enormous for thick beams and less significant for thin beams. Lastly, a comprehensive 3D interaction diagram of the natural frequencies, temperature and material parameters is plotted in Fig. 9. With a specific value of p, the natural frequencies of ZrO_2/SUS304 beams are smaller than those of Si_3N_4/SUS304 beams at the same temperature.

4. Conclusions

Analytical solutions based on the state space approach are developed to study vibration and buckling behaviours of FG beams under mechanical/thermal loads using a high-order beam theory. Equations of motion derived from Hamilton's principle. The natural frequencies, critical buckling loads, critical temperatures, load-frequency curves and temperature-frequencies curves of FG beams are investigated. The results obtained from temperature dependent solution are significantly lower than those of temperature independent one especially for thick beams. The effects of temperature distribution through the thickness on natural frequencies and critical temperatures are also investigated. The present model is found to be appropriate and efficient in analysing the vibration and buckling of FG beams under mechanical/ thermal loads.

References

1. Şimşek M, Kocatürk T. Free and forced vibration of a functionally graded beam subjected to a concentrated moving harmonic load. Composite Structures. 2009;90(4):465-73.

2. Şimşek M. Fundamental frequency analysis of functionally graded beams by using different higher-order beam theories. Nuclear Engineering and Design. 2010;240(4):697-705.

3. Pradhan KK, Chakraverty S. Free vibration of Euler and Timoshenko functionally graded beams by Rayleigh–Ritz method. Composites Part B: Engineering. 2013;51:175-84.

4. Pradhan KK, Chakraverty S. Generalized power-law exponent based shear deformation theory for free vibration of functionally graded beams. Applied Mathematics and Computation. 2015;268:1240-58.

5. Su H, Banerjee JR. Development of dynamic stiffness method for free vibration of functionally graded Timoshenko beams. Computers & Structures. 2015;147:107-16.

6. Su H, Banerjee JR, Cheung CW. Dynamic stiffness formulation and free vibration analysis of functionally graded beams. Composite Structures. 2013;106:854-62.

7. Wattanasakulpong N, Mao Q. Dynamic response of Timoshenko functionally graded beams with classical and non-classical boundary conditions using Chebyshev collocation method. Composite Structures. 2015;119:346-54.

8. Vo TP, Thai H-T, Nguyen T-K, Inam F, Lee J. Static behaviour of functionally graded sandwich beams using a quasi-3D theory. Composites Part B: Engineering. 2015;68:59-74.

9. Vo TP, Thai H-T, Nguyen T-K, Inam F, Lee J. A quasi-3D theory for vibration and buckling of functionally graded sandwich beams. Composite Structures. 2015;119:1-12.

10. Vo TP, Thai H-T, Nguyen T-K, Maheri A, Lee J. Finite element model for vibration and buckling of functionally graded sandwich beams based on a refined shear deformation theory. Engineering Structures. 2014;64:12-22.

11. Jin C, Wang X. Accurate free vibration analysis of Euler functionally graded beams by the weak form quadrature element method. Composite Structures. 2015;125:41-50.

12. Filippi M, Pagani A, Petrolo M, Colonna G, Carrera E. Static and free vibration analysis of laminated beams by refined theory based on Chebyshev polynomials. Composite Structures. 2015;132:1248-59.

13. Mashat DS, Carrera E, Zenkour AM, Al Khateeb SA, Filippi M. Free vibration of FGM layered beams by various theories and finite elements. Composites Part B: Engineering. 2014;59:269-78.

14. Fazzolari FA. Stability analysis of FGM sandwich plates by using variable-kinematics Ritz models. Mechanics of Advanced Materials and Structures. 2016;23(9):1104-13.

15. Tornabene F, Fantuzzi N, Bacciocchi M, Viola E. Effect of agglomeration on the natural frequencies of functionally graded carbon nanotube-reinforced laminated composite doubly-curved shells. Composites Part B: Engineering. 2016;89:187-218.

16. Aydogdu M, Taskin V. Free vibration analysis of functionally graded beams with simply supported edges. Materials & Design. 2007;28(5):1651-6.

17. Giunta G, Crisafulli D, Belouettar S, Carrera E. Hierarchical theories for the free vibration analysis of functionally graded beams. Composite Structures. 2011;94(1):68-74.

18. Thai H-T, Vo TP. Bending and free vibration of functionally graded beams using various higher-order shear deformation beam theories. International Journal of Mechanical Sciences. 2012;62(1):57-66.

19. Nguyen T-K, Vo TP, Thai H-T. Static and free vibration of axially loaded functionally graded beams based on the first-order shear deformation theory. Composites Part B: Engineering. 2013;55:147-57.

20. Nguyen T-K, Nguyen TT-P, Vo TP, Thai H-T. Vibration and buckling analysis of functionally graded sandwich beams by a new higher-order shear deformation theory. Composites Part B: Engineering. 2015;76:273-85.

21. Khdeir AA. Dynamic response of antisymmetric cross-ply laminated composite beams with arbitrary boundary conditions. Int Z Engng Sci. 1996;34(1):9-19.

22. Khdeir AA. Forced Vibration of Antisymmetric Angle-Ply Laminated Plates with Various Boundary Conditions. Journal of Sound and Vibration. 1995;188(2):257-67.

23. Khdeir AA, Reddy JN. An exact solution for the bending of thin and thick cross-ply laminated beams. Composite Structures. 1997;37:195-203.

24. Sina SA, Navazi HM, Haddadpour H. An analytical method for free vibration analysis of functionally graded beams. Materials & Design. 2009;30(3):741-7.

25. Trinh LC, Vo TP, Osofero AI, Lee J. Fundamental frequency analysis of functionally graded sandwich beams based on the state space approach. Composite Structures. 2015;DOI:10.1016/j.compstruct.2015.11.010.

26. Sankar BV, Tzeng JT. Thermal Stresses in Functionally Graded Beams. AIAA Journal. 2002;40(6):1228-32.

27. Malekzadeh P, Monajjemzadeh SM. Dynamic response of functionally graded beams in a thermal environment under a moving load. Mechanics of Advanced Materials and Structures. 2015;23(3):248-58.

28. Esfahani SE, Kiani Y, Eslami MR. Non-linear thermal stability analysis of temperature dependent FGM beams supported on non-linear hardening elastic foundations International Journal of Mechanical Sciences. 2013;69:10-20.

29. Ghiasian SE, Kiani Y, Eslami MR. Nonlinear thermal dynamic buckling of FGM beams. European Journal of Mechanics - A/Solids. 2015;54:232-42.

30. Sun Y, Li S-R, Batra RC. Thermal buckling and post-buckling of FGM Timoshenko beams on nonlinear elastic foundation. Journal of Thermal Stresses. 2016;39(1):11-26.

31. Wattanasakulpong N, Gangadhara Prusty B, Kelly DW. Thermal buckling and elastic vibration of third-order shear deformable functionally graded beams. International Journal of Mechanical Sciences. 2011;53(9):734-43.

32. Giunta G, Crisafulli D, Belouettar S, Carrera E. A thermo-mechanical analysis of functionally graded beams via hierarchical modelling. Composite Structures. 2013;95:676-90.

33. Shen H-S, Wang Z-X. Nonlinear analysis of shear deformable FGM beams resting on elastic foundations in thermal environments. International Journal of Mechanical Sciences. 2014;81:195-206.

34. Khdeir AA, Reddy JN. Free vibration of cross-ply laminated beams with arbitrary boundary conditions. International Journal of Engineering Science. 1994;32(12):1971-80.

35. Ebrahimi F, Salari E. Thermal buckling and free vibration analysis of size dependent Timoshenko FG nanobeams in thermal environments. Composite Structures. 2015;128:363-80.

36. Reddy JN, Chin CD. Thermomechanical Analysis of Functionally Graded Cylinders and Plates. Journal of Thermal Stresses. 1998;21(6):593-626.

37. Li S-R, Batra RC. Relations between buckling loads of functionally graded Timoshenko and homogeneous Euler–Bernoulli beams. Composite Structures. 2013;95:5-9.

38. Ebrahimi F, Salari E. Nonlocal thermo-mechanical vibration analysis of functionally graded nanobeams in thermal environment. Acta Astronautica. 2015;113:29-50.

LIST OF TABLES

Table 1: Temperature-dependent coefficients for ceramics and metals [33, 36].

Table 2: The first five natural frequencies of Al_2O_3/Fe beam $(a/h = 5, \upsilon = 0.23)$.

Table 3: The first five natural frequencies of Al_2O_3/Al beams $(a/h = 5, \upsilon = 0.3)$.

Table 4: The first five natural frequencies of Al_2O_3/Al beams $(a/h = 20, \upsilon = 0.3)$.

Table 5: Dimensionless critical buckling loads of Al_2O_3/Al beams $(\upsilon = 0.23)$.

Table 6: Dimensionless critical temperatures of Al_2O_3/SUS304 beams under UTR $(p = 0.3)$.

Table 7: The critical temperatures of various FG beams under UTR $(a/h = 30)$.

Table 8: Fundamental frequency with respect to the temperature rise of Al_2O_3/SUS304 beams

Table 9: The critical temperatures of Si_3N_4/SUS304 beams under UTR and LNR.

Table 10: Dimensionless natural frequencies of $P-P$ Si_3N_4/SUS304 beams under UTR and LNR $(a/h = 20)$.

Table 11: Fundamental frequency of Si_3N_4/SUS304 beams under LNR and NLNR $(a/h = 20)$.

Table 12: The critical temperatures of various FG beams under LNR and NLTR with various material parameters $(a/h = 20)$.

LIST OF FIGURES

Fig. 1: Coordinates of FG beam and temperature distributions.

Fig. 2: Young's modulus and thermal expansion of ceramics and metals with respect to the temperature change.

Fig. 3: The effect of material parameters on the first load – frequency curves of $C-C$ Al_2O_3/Al beams $(a/h=5)$.

Fig. 4. The first five load – frequency curves of $C-C$ Al_2O_3/Al beams $(p=0.5)$.

Fig. 5: Temperature distributions and Young's modulus of Si_3N_4/SUS304 beams through the thickness with $\Delta T=0$ and 900K.

Fig. 6: The first temperature – frequency curves of $C-C$ FG beams $(a/h=20)$.

Fig. 7: The effect of material parameters on the critical temperatures of various FG beams under LNR $(C-P, a/h=20)$.

Fig. 8: The effect of slenderness ratios on the critical temperatures of $C-P$ Si_3N_4/SUS304 beam under UTR, LNR and NLNR $(p=0.5)$.

Fig. 9: Frequency – temperature – material parameter interaction curves of Si_3N_4/SUS304 and ZrO_2/SUS304 beams under NLNR.

Table 1: Temperature-dependent coefficients for ceramics and metals [33, 36].

Materials	Proprieties	P_0	P_{-1}	P_1	P_2	P_3
ZrO_2	$E(Pa)$	244.27e+9	0.0	−1.371e−3	1.214e−6	−3.681e−10
	$\alpha(1/K)$	12.766e−6	0.0	−1.491e−3	1.006e−5	−6.778e−11
	$\kappa(W/mK)$	1.7	0.0	1.276e−4	6.648e−8	0.0
	υ	0.2882	0.0	1.133e−4	0.0	0.0
	$\rho(kg/m^3)$	3000	0.0	0.0	0.0	0.0
Ti–6Al–4V	$E(Pa)$	122.56e+9	0.0	−4.586e−4	0.0	0.0
	$\alpha(1/K)$	7.5788e−6	0.0	6.638e−4	−3.147e−6	0.0
	$\kappa(W/mK)$	1	0.0	1.704e−2	0.0	0.0
	υ	0.2884	0.0	1.121e−4	0.0	0.0
	$\rho(kg/m^3)$	4429	0.0	0.0	0.0	0.0
Al_2O_3	$E(Pa)$	349.55e+9	0.0	−3.853e−4	4.027e−7	−1.673e−10
	$\alpha(1/K)$	6.8269e−6	0.0	1.838e−4	0.0	0.0
	$\kappa(W/mK)$	0.26	0.0	0.0	0.0	0.0
	υ	3800	0.0	0.0	0.0	0.0
Si_3N_4	$E(Pa)$	348.43e+9	0.0	−3.070e−4	2.160e−7	−8.946e−11
	$\alpha(1/K)$	5.8723e−6	0.0	9.095e−4	0.0	0.0
	$\kappa(W/mK)$	13.723	0.0	−1.032e−3	5.466e−7	−7.876e−11
	υ	0.24	0.0	0.0	0.0	0.0
	$\rho(kg/m^3)$	2370	0.0	0.0	0.0	0.0
SUS304	$E(Pa)$	201.04e+9	0.0	3.079e−4	−6.534e−7	0.0
	$\alpha(1/K)$	12.330e−6	0.0	8.086e−4	0.0	0.0
	$\kappa(W/mK)$	15.379	0.0	−1.264e−3	2.092e−6	−7.223e−10
	υ	0.3262	0.0	−2.002e−4	3.797e−7	0.0
	$\rho(kg/m^3)$	8166	0.0	0.0	0.0	0.0

Table 2: The first five natural frequencies of Al_2O_3/Fe beam $(a/h = 5, \upsilon = 0.23)$.

BCs	Mode	HOBT [4]			Present		
		p = 0	1	5	p = 0	1	5
C–C	1	10.1083	7.1931	5.9855	10.0900	7.1792	5.9733
	2	23.4657	16.6790	13.7711	23.3851	16.6227	13.7217
	3	30.1621	21.6365	17.5660	30.0429	21.5514	17.4969
	4	39.5482	28.1168	23.1248	39.3343	27.9666	22.9966
	5	56.9319	40.5008	33.2252	56.6051	40.2698	33.0330
C–P	1	7.4965	5.3367	4.4732	7.4820	5.3258	4.4630
	2	20.8194	14.7529	12.2782	20.7202	14.6850	12.2137
	3	30.1051	21.5866	17.5253	30.0429	21.5411	17.4888
	4	37.1746	26.3968	21.8323	36.9144	26.2154	21.6648
	5	55.0385	39.1297	32.2220	54.5653	38.7958	31.9196
P-P	1	5.1421	3.6904	3.1102	5.1328	3.6838	3.1036
	2	17.9856	12.6934	10.6599	17.8919	12.6305	10.5962
	3	30.0429	21.5385	17.4859	30.0429	21.5363	17.4851
	4	34.6496	24.5556	20.4458	34.3664	24.3597	20.2538
	5	52.9685	37.6354	31.1266	52.4237	37.2521	30.7598
C-F	1	1.8859	1.3370	1.1330	1.8856	1.3366	1.1328
	2	10.2557	7.2519	6.0953	10.2424	7.2424	6.0869
	3	15.0556	10.8759	8.8021	15.0215	10.8509	8.7820
	4	24.6380	17.4526	14.5612	24.5760	17.4088	14.5232
	5	41.2404	29.2206	24.2486	41.0964	29.1177	24.1625

Table 3: The first five natural frequencies of Al_2O_3/Al beams $(a/h = 5, \upsilon = 0.3)$.

BCs	Mode	Theory	p						
			0	0.2	0.5	1	2	5	10
C-C	1	Present	10.0670	9.4610	8.7430	7.9479	7.1749	6.4920	6.1637
		HOBT [4]	10.0858	9.4789	8.7614	7.9680	7.1963	6.5120	6.1809
		HOBT [10]	9.9984	9.3834	–	7.1905	7.1901	6.6447	6.3161
	2	Present	23.2348	21.9426	20.3696	18.5535	16.6326	14.6873	13.8331
		HOBT [4]	23.1004	21.7700	20.2077	18.4654	16.7457	15.2301	14.3617
		HOBT [10]	23.8754	22.4840	–	19.0494	17.2924	15.7868	14.9035
	3	Present	30.2314	28.8710	27.2560	25.2965	22.8618	19.7959	18.1426
		HOBT [4]	30.3513	28.9837	27.3569	25.3859	22.9576	19.9122	18.2304
		HOBT [10]	30.2391	28.8837	–	25.3746	23.0112	19.9634	18.2321
	4	Present	38.9966	36.9209	34.3634	31.3450	28.0113	24.4518	22.9386
		HOBT [4]	38.6867	36.5446	34.0075	31.1243	28.1712	25.4176	23.8724
		HOBT [10]	38.1841	36.0793	–	30.7500	27.8331	25.0901	23.5501
	5	Present	56.0388	53.1438	49.5539	45.2610	40.3898	34.9988	32.7237
C-P	1	Present	7.4872	7.0190	6.4853	5.9194	5.3973	4.9555	4.7096
	2	Present	20.6436	19.4245	17.9412	16.2594	14.5784	13.0744	12.4237
	3	Present	30.2314	28.8346	27.0942	24.9211	22.3225	19.4312	17.9731
	4	Present	36.6649	34.6508	32.2123	29.4057	26.3838	23.2037	21.8094
	5	Present	54.0805	51.2108	47.6537	43.4538	38.8345	33.8788	31.7447
P-P	1	Present	5.1528	4.8373	4.5328	4.2551	4.0060	3.7055	3.4513
		HOBT [4]	5.1629	4.8459	4.5405	4.2632	4.0165	3.7178	3.4617
		HOBT [2]	5.1527	4.8092	4.4111	3.9904	3.6264	3.4012	3.2816
	2	Present	17.8812	16.7457	15.3460	13.7721	12.2950	11.2435	10.8417
		HOBT [4]	17.8908	16.7317	15.3306	13.7778	12.3619	11.4822	11.1126
		HOBT [18]	17.8812	–	15.4588	14.0100	12.6405	11.5431	11.0240
	3	Present	30.2314	28.8216	27.0409	24.8044	22.1397	19.2751	17.8986
		HOBT [4]	30.2314	28.8311	27.0804	24.9042	22.3517	19.5600	18.0553
	4	Present	34.2097	32.2316	29.8178	27.0642	24.2724	21.6679	20.5189
		HOBT [4]	34.2103	32.1672	29.7504	27.0657	24.4881	22.4290	21.3110
	(3^{rd})	HOBT [18]	34.2097	–	29.8382	27.0979	24.3152	21.7158	20.5561
	5	Present	52.0266	49.2114	45.7758	41.7866	37.4666	32.8483	30.8097
C-F	1	Present	1.8952	1.7659	1.6180	1.4633	1.3325	1.2592	1.2183
		HOBT [4]	1.8955	1.7663	1.6187	1.4645	1.3341	1.2605	1.2192
		HOBT [2]	1.8952	1.7664	1.6182	1.4633	1.3325	1.2592	1.2183
	2	Present	10.2449	9.6009	8.8376	8.0000	7.2165	6.6126	6.3329
	3	Present	15.1157	14.4405	13.6509	12.7064	11.5380	10.0175	9.1418
	4	Present	24.4943	23.0540	21.3108	19.3344	17.3571	15.5929	14.8146
	5	Present	40.8428	38.5697	35.7680	32.5036	29.0633	25.7015	24.2665

Table 4: The first five natural frequencies of Al_2O_3/Al beams $\left(a/h = 20, \upsilon = 0.3\right)$.

BCs	Mode	Theory	p						
			0	0.2	0.5	1	2	5	10
C-C	1	Present	12.2220	11.3829	10.4264	9.4304	8.5964	8.1433	7.8843
		HOBT [4]	12.2256	11.3873	10.4344	9.4438	8.6138	8.1587	7.8947
		HOBT [2]	12.2238	11.3873	10.4287	9.4316	8.5975	8.1446	7.8858
	2	Present	32.9847	30.7531	28.1961	25.5135	23.2256	21.8774	21.1323
		HOBT [4]	33.0067	30.7650	28.2156	25.5579	23.3181	22.0692	21.3200
		HOBT [10]	33.1335	30.8452	–	25.6223	23.3691	22.1345	21.4015
	3	Present	62.9501	58.7652	53.9394	48.8302	44.3784	41.5305	40.0120
	4	Present	100.8042	94.2319	86.5989	78.4340	71.1524	66.1173	63.5259
	5	Present	120.9255	115.5023	109.1142	101.4369	91.9532	79.7556	72.8650
C-P	1	Present	8.4818	7.9048	7.2661	6.6185	6.0825	5.7590	5.5394
	2	Present	27.0325	25.1934	23.1060	20.9382	19.1105	18.0472	17.4270
	3	Present	55.0943	51.3918	47.1428	42.6752	38.8332	36.4777	35.1962
	4	Present	91.5210	85.4580	78.4155	70.9138	64.3101	59.9881	57.8131
	5	Present	120.9255	115.3858	108.4948	99.7472	89.6828	78.6828	72.4547
P-P	1	Present	5.4603	5.1145	4.7882	4.5023	4.2679	4.0062	3.7385
		HOBT [4]	5.4606	5.1147	4.7884	4.5024	4.2682	4.0064	3.7386
		HOBT [2]	5.4603	5.0829	4.6516	4.2050	3.8361	3.6485	3.5390
	2	Present	21.5733	20.0862	18.3863	16.6132	15.1294	14.3430	13.9072
		HOBT [4]	21.5755	20.0852	18.3849	16.6146	15.1402	14.3804	13.9476
		HOBT [18]	21.5732	–	18.3962	16.6344	15.1619	14.3746	13.9263
	3	Present	47.5930	44.3860	40.7701	37.0322	33.8617	31.8877	30.7013
		HOBT [4]	47.6037	44.3818	40.7639	37.0394	33.9159	32.0700	30.8925
		HOBT [18]	47.5930	–	40.6526	36.7679	33.4689	31.5780	30.5369
	4	Present	82.4440	76.8748	70.3592	63.4075	57.3561	53.7341	52.0589
	5	Present	120.9255	115.3797	107.1710	97.0194	88.0267	78.5197	72.3662
C-F	1	Present	1.9496	1.8142	1.6603	1.5011	1.3696	1.3034	1.2645
		HOBT [4]	1.9496	1.8143	1.6609	1.5021	1.3711	1.3046	1.2653
		HOBT [2]	1.9495	1.8146	1.6605	1.5011	1.3696	1.3033	1.2645
	2	Present	12.0763	11.2437	10.2952	9.3090	8.4866	8.0519	7.8031
	3	Present	33.2090	30.9454	28.3548	25.6435	23.3493	22.0546	21.3370
	4	Present	60.4627	57.7450	54.1826	49.0669	44.5516	39.8371	36.4295
	5	Present	63.4715	59.2190	54.6881	50.7995	46.1233	42.0226	40.5138

Table 5: Dimensionless critical buckling loads of Al_2O_3/Al beams $(\upsilon = 0.23)$.

a/h	BCs	Theory	p					
			0	0.5	1	2	5	10
5	C-C	Present	154.534	103.732	80.566	61.733	47.468	41.759
		HOBT [10]	154.550	103.732	80.609	61.793	47.756	41.804
		FOBT [37]	154.350	103.220	80.498	62.614	50.384	44.267
	C-P	Present	90.022	59.500	46.107	35.568	28.387	25.203
		FOBT [37]	97.580	64.052	49.497	38.576	32.000	28.731
	P-P	Present	48.648	31.987	24.648	19.109	15.664	14.098
		HOBT [10]	48.840	32.009	24.691	19.161	15.740	14.147
		FOBT [37]	48.835	31.967	24.687	19.245	16.024	14.427
	C-F	Present	13.043	8.293	6.500	4.931	4.270	3.848
		HOBT [10]	13.077	8.502	6.543	5.098	4.278	3.882
		FOBT [37]	13.213	8.578	6.600	5.150	4.345	3.950
10	C-C	Present	195.179	127.876	98.625	76.622	62.902	56.431
		HOBT [10]	195.361	128.050	98.787	76.668	62.979	56.597
		FOBT [37]	195.340	127.870	98.749	76.980	61.062	57.708
	C-P	Present	103.596	67.284	51.264	40.584	33.108	29.904
		FOBT [37]	106.330	69.154	52.251	41.535	33.436	31.705
	P-P	Present	52.204	33.478	26.102	19.860	17.023	15.321
		HOBT [10]	52.308	34.009	26.173	20.394	17.112	15.529
		FOBT [37]	52.309	33.996	26.171	20.416	17.192	15.612
	C-F	Present	13.173	8.523	6.586	5.037	4.262	3.874
		HOBT [10]	13.374	8.671	6.668	5.203	4.398	4.005
		FOBT [37]	13.349	8.657	6.657	5.194	4.209	3.997

Table 6: Dimensionless critical temperatures of Al_2O_3/SUS304 beams under UTR $\left(p=0.3\right)$.

	a/h	20			40		
	BCs	C-C	C-P	P-P	C-C	C-P	P-P
TID	HOBT [31]	4.1231	2.1418	1.0650	4.2251	2.1740	1.0685
	Present	4.1545	2.4206	1.1319	4.2349	2.2709	1.0861
TD	HOBT [31]	3.4279	1.9274	1.0036	3.9992	2.1081	1.0527
	Present	3.4246	1.9165	0.9924	3.9695	2.0902	1.0353

Table 7: The critical temperatures of various FG beams under UTR $(a/h = 30)$.

BCs	Materials	Theory	TID				TD			
			p = 0	1	5	10	p = 0	1	5	10
P-P	Si_3N_4/SUS304	HOBT [31]	1.348	0.876	0.750	0.712	1.185	0.805	0.697	0.664
		Present	1.307	0.866	0.744	0.710	1.151	0.796	0.693	0.663
	Al_2O_3/SUS304	HOBT [31]	1.376	0.880	0.747	0.708	1.326	0.827	0.698	0.662
		Present	1.347	0.870	0.740	0.705	1.296	0.817	0.694	0.661
	ZrO_2/SUS304	HOBT [31]	0.518	0.565	0.589	0.600	0.416	0.481	0.530	0.549
		Present	0.514	0.562	0.588	0.600	0.414	0.479	0.529	0.549
	ZrO_2/Ti-6Al-4V	Present	0.514	0.715	1.091	1.227	0.414	0.583	1.003	8.104
C-P	Si_3N_4/SUS304	Present	2.654	1.758	1.510	1.440	2.115	1.503	1.321	1.267
	Al_2O_3/SUS304	Present	2.732	1.767	1.502	1.430	2.526	1.567	1.329	1.267
	ZrO_2/SUS304	Present	1.042	1.143	1.194	1.217	0.715	0.850	0.977	1.029
	ZrO_2/Ti-6Al-4V	Present	1.042	1.453	2.212	2.489	0.715	1.009	1.865	9.285
C-C	Si_3N_4/SUS304	Present	5.130	3.398	2.917	2.782	3.559	2.609	2.333	2.244
	Al_2O_3/SUS304	Present	5.280	3.415	2.902	2.763	4.540	2.769	2.364	2.254
	ZrO_2/SUS304	Present	2.013	2.207	2.309	2.352	1.117	1.363	1.642	1.762
	ZrO_2/Ti-6Al-4V	Present	2.013	2.809	4.269	4.806	1.117	1.570	3.070	8.104

Table 8: Fundamental frequency with respect to the temperature rise of Al_2O_3/SUS304 beams under UTR $(a/h = 20)$.

			p = 0.2			p = 2		
	BCs	Theory	ΔT = 0	50	100	ΔT = 0	50	100
TID	C-C	HOBT [31]	6.6394	6.1189	5.5452	6.7355	5.9802	5.1028
		Present	6.6371	6.1209	5.5489	6.7366	5.9834	5.1125
	C-P	Present	4.5898	3.8574	2.9297	4.6653	3.5731	1.8925
	P-P	Present	2.9506	1.8450	-	3.0129	1.1816	-
TD	C-C	HOBT [31]	6.6394	6.1109	5.5081	6.7335	5.9581	4.9965
		Present	6.6371	6.1142	5.5141	6.7366	5.9631	5.0068
	C-P	Present	4.5898	3.8437	2.8608	4.6653	3.5391	1.5946
	P-P	Present	2.9506	1.8220	-	3.0129	1.0868	-

Table 9: The critical temperatures of Si_3N_4/SUS304 beams under UTR and LNR.

a/h	BCs	Theory	UTR			LNR		
			p = 0	1	5	p = 0	1	5
40	P-P	Present	51.72	34.69	29.95	125.00	85.94	71.88
		FOBT [35]	–	–	–	127.33	84.62	69.43
	C-P	Present	102.02	69.26	59.96	246.88	175.00	146.88
	C-C	Present	187.87	129.87	113.01	451.56	328.13	279.69
20	P-P	Present	187.88	129.87	113.01	451.56	328.13	279.69
	C-P	Present	345.14	245.24	215.51	814.06	612.50	531.25
	C-C	Present	580.66	425.69	380.61	–*	1062.50	957.81

(–*) This value does not exist since the critical temperature of FG beams is higher than the melting point $\left(E_m = 0\right)$

Table 10: Dimensionless natural frequencies of $P-P$ Si_3N_4/SUS304 beams under UTR and LNR $(a/h=20)$.

ΔT	Mode	Theory	UTR			LNR		
			p=0	1	5	p=0	1	5
10	1	FOBT [35]	–	–	–	9.6461	5.7717	4.6925
		Present	2.8842	2.7347	2.4845	9.6843	5.8432	4.7454
	2	FOBT [35]	–	–	–	38.6688	23.2890	19.0001
		Present	11.5991	11.4594	11.2261	38.6698	23.2942	19.0058
	3	FOBT [35]	–	–	–	85.5816	51.5787	42.0838
		Present	25.6350	25.5020	25.2740	85.4928	51.5782	42.0626
30	1	FOBT [35]	–	–	–	9.4538	5.6105	4.5363
		Present	2.8450	2.6157	2.2158	9.4864	5.6727	4.5792
	2	FOBT [35]	–	–	–	38.4794	23.1492	18.8693
		Present	11.4678	11.2543	10.9045	38.4431	23.1103	18.8315
	3	FOBT [35]	–	–	–	85.3911	51.4659	41.9855
		Present	25.4240	25.2178	24.8745	85.2146	51.3662	41.8680
60	1	FOBT [35]	–	–	–	9.1475	5.3537	4.2875
		Present	2.9109	2.6325	2.1295	9.1774	5.4030	4.3136
	2	FOBT [35]	–	–	–	38.1838	22.9319	18.6672
		Present	11.8148	11.5484	11.1378	38.0975	22.8282	18.5625
	3	FOBT [35]	–	–	–	85.0946	51.2893	41.8321
		Present	26.1669	25.9057	25.4947	84.7945	51.0434	41.5692

Table 11: Fundamental frequency of Si_3N_4/SUS304 beams under LNR and NLNR $(a/h = 20)$.

BCs	Temperature distribution	ΔT(K) = 20			40			80		
		p=0.1	0.5	1	p=0.1	0.5	1	p=0.1	0.5	1
C-C	LNR [38]	19.6398	15.2580	13.3671	19.5436	15.1759	13.2905	19.3420	15.0040	13.1304
	Present	19.3371	15.0222	13.1554	19.2191	14.9156	13.0533	18.9778	14.6972	12.8431
	NLNR [38]	19.6390	15.2501	13.3558	19.5449	15.1635	13.2715	19.3552	14.9886	13.1011
	Present	19.3379	15.0244	13.1579	19.2211	14.9212	13.0597	18.9832	14.7115	12.8600
C-P	LNR [38]	13.4380	10.4238	9.1227	13.3037	10.3040	9.0082	13.0201	10.0515	8.7674
	Present	13.3373	10.3526	9.0635	13.1893	10.2165	8.9317	12.8837	9.9342	8.6571
	NLNR [38]	13.4395	10.4211	9.1178	13.3105	10.3020	9.0018	13.0483	10.0594	8.7648
	Present	13.3382	10.3553	9.0669	13.1920	10.2237	8.9404	12.8907	9.9533	8.6801
P-P	LNR [38]	8.4634	6.5415	5.7114	8.2781	6.3717	5.5469	7.8795	6.0063	5.1927
	Present	8.4716	6.5742	5.7588	8.2802	6.3957	5.5847	7.8766	6.0166	5.2128
	NLNR [38]	8.4675	6.5437	5.7124	8.2911	6.3803	5.5527	7.9265	6.0402	5.2186
	Present	8.4730	6.5779	5.7632	8.2837	6.4055	5.5965	7.8861	6.0431	5.2448

Table 12: The critical temperatures of various FG beams under LNR and NLTR with various material parameters $(a/h = 20)$.

BCs	Materials	Temperature distribution	p					
			0	0.5	1	2	5	10
C-C	Si_3N_4/SUS304	LNR	-	1142.19	1062.50	1004.69	957.81	921.88
		NLNR	-	-	-	1132.50	1042.50	972.50
	ZrO_2/SUS304	LNR	390.74	421.17	438.14	465.66	521.28	583.24
		NLNR	390.74	492.47	532.42	565.64	605.16	642.05
	ZrO_2/Ti-6Al-4V	LNR	390.40	404.79	431.43	484.90	625.60	828.12
		NLNR	390.40	449.57	484.92	539.57	668.54	853.83
C-P	Si_3N_4/SUS304	LNR	814.06	667.19	612.50	570.31	531.25	507.81
		NLNR	814.06	736.25	688.75	637.50	572.50	531.25
	ZrO_2/SUS304	LNR	258.41	279.66	289.76	305.47	336.40	365.50
		NLNR	258.41	330.88	357.72	377.09	393.99	406.30
	ZrO_2/Ti-6Al-4V	LNR	259.23	268.78	286.47	325.85	428.52	565.48
		NLNR	259.23	302.11	325.87	366.91	461.02	587.44
P-P	Si_3N_4/SUS304	LNR	451.56	360.94	328.13	301.56	279.69	265.63
		NLNR	451.56	388.75	357.50	327.50	293.75	273.75
	ZrO_2/SUS304	LNR	155.05	167.79	173.86	179.21	192.87	204.68
		NLNR	155.05	201.63	216.12	227.83	230.85	231.72
	ZrO_2/Ti-6Al-4V	LNR	155.54	163.42	174.17	200.72	263.97	343.81
		NLNR	155.54	183.68	200.73	228.95	287.68	361.86

(-) These values do not exist since the critical temperature of FG beams is higher than the melting point $(E_m = 0)$

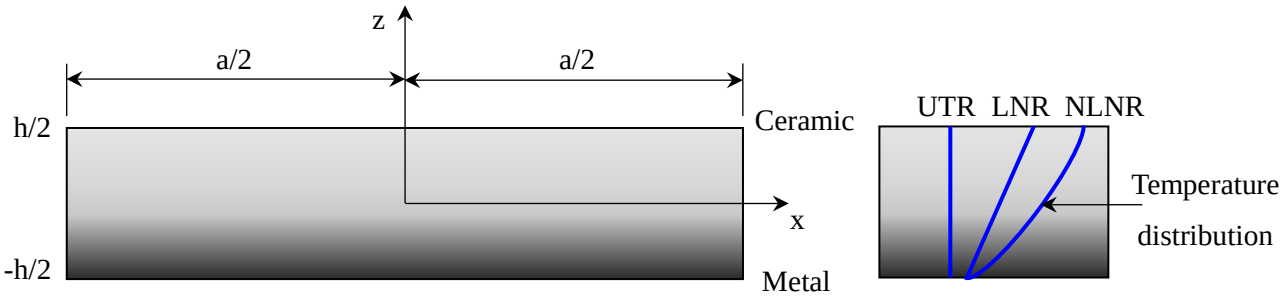

Fig. 1: Coordinates of FG beam and temperature distributions.

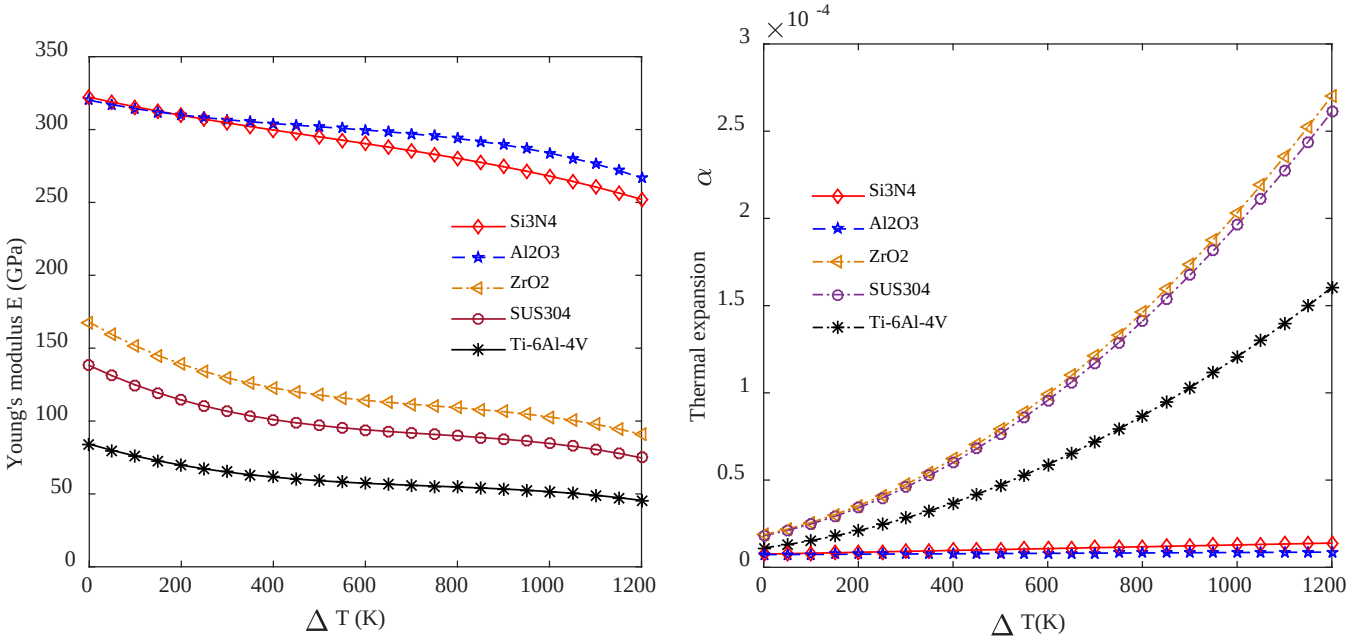

Fig. 2: Young's modulus and thermal expansion of ceramics and metals with respect to the temperature change.

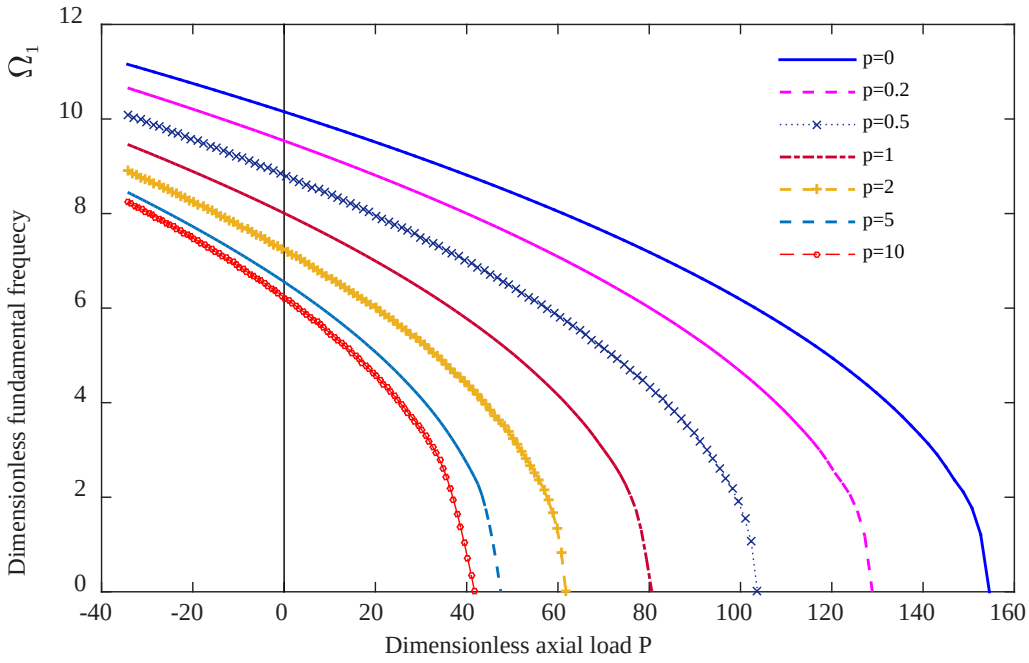

Fig. 3: The effect of material parameters on the first load – frequency curves of $C-C$ Al_2O_3/Al beams $(a/h=5)$.

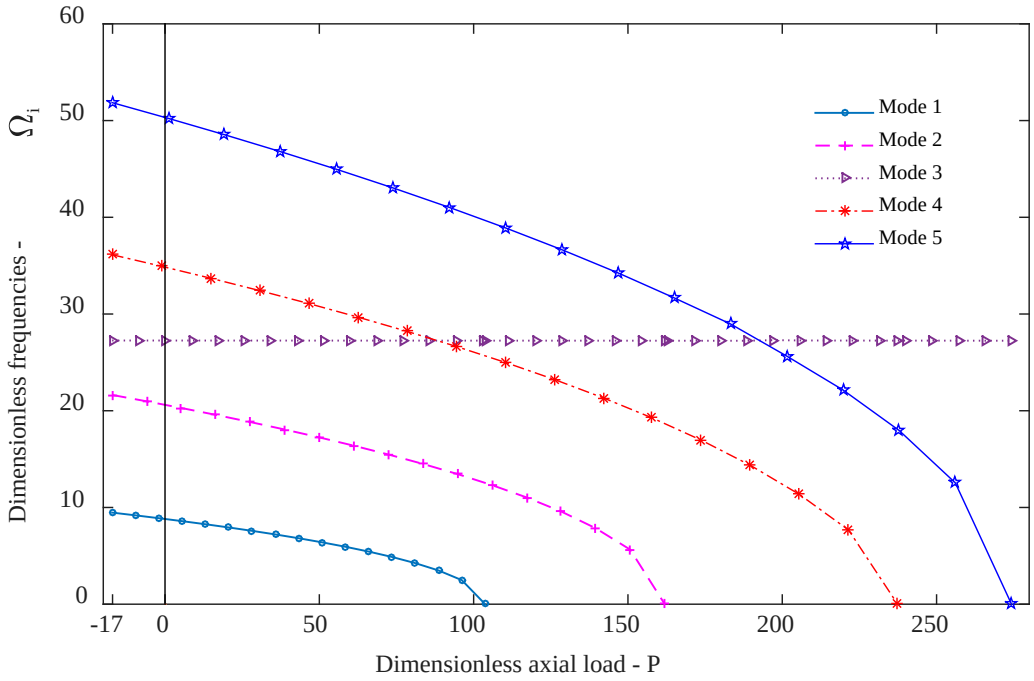

a) $a/h = 5$

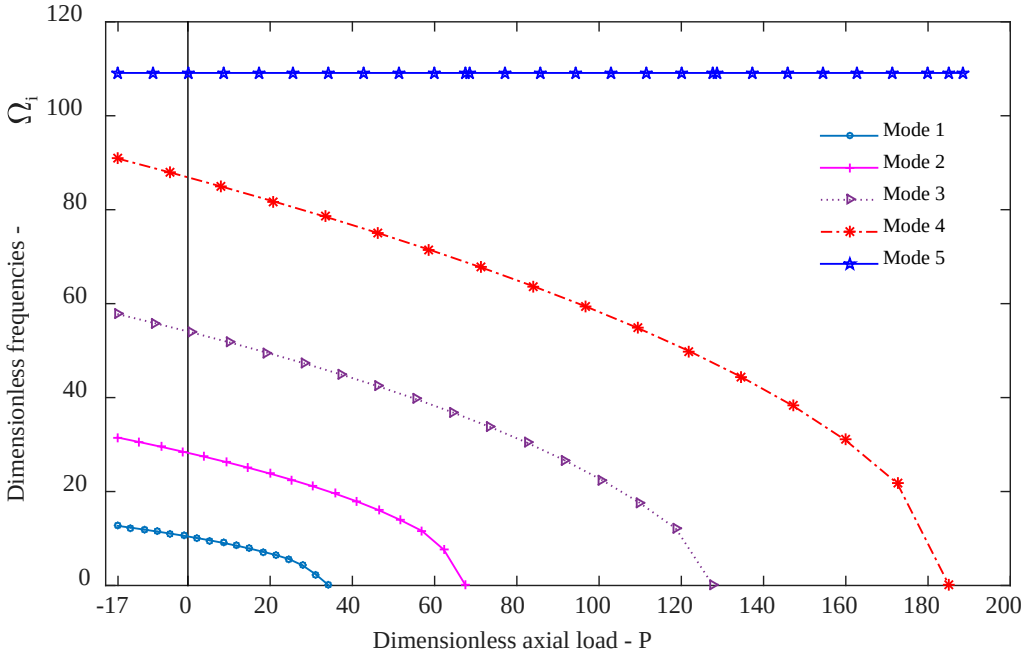

b) $a/h = 20$

Fig. 4. The first five load – frequency curves of $C-C$ Al_2O_3/Al beams $(p = 0.5)$.

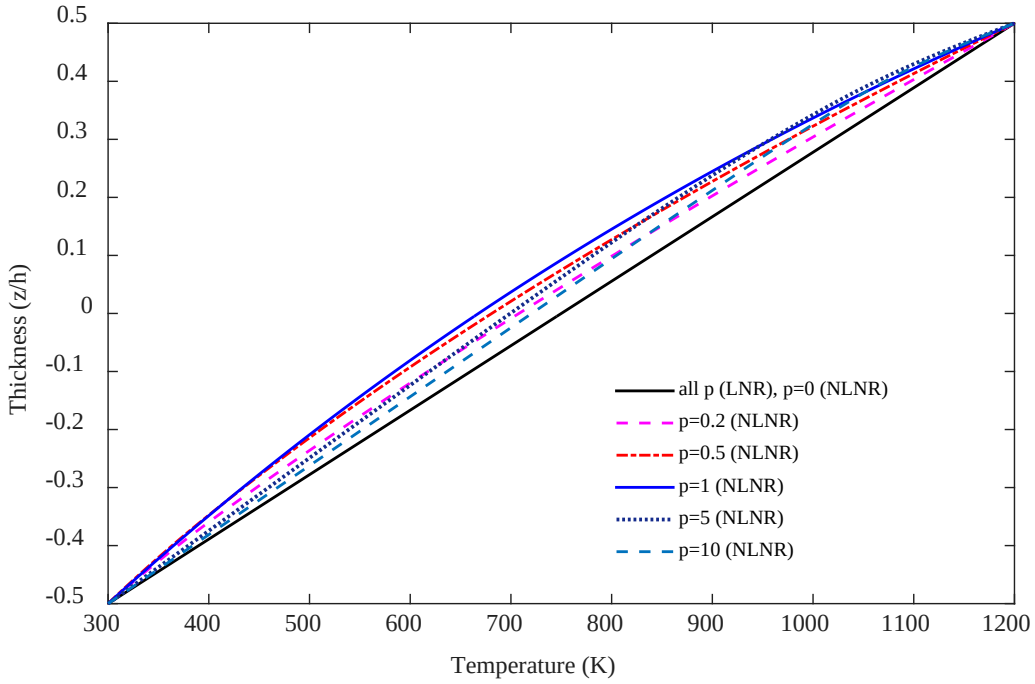

a) Temperature distributions.

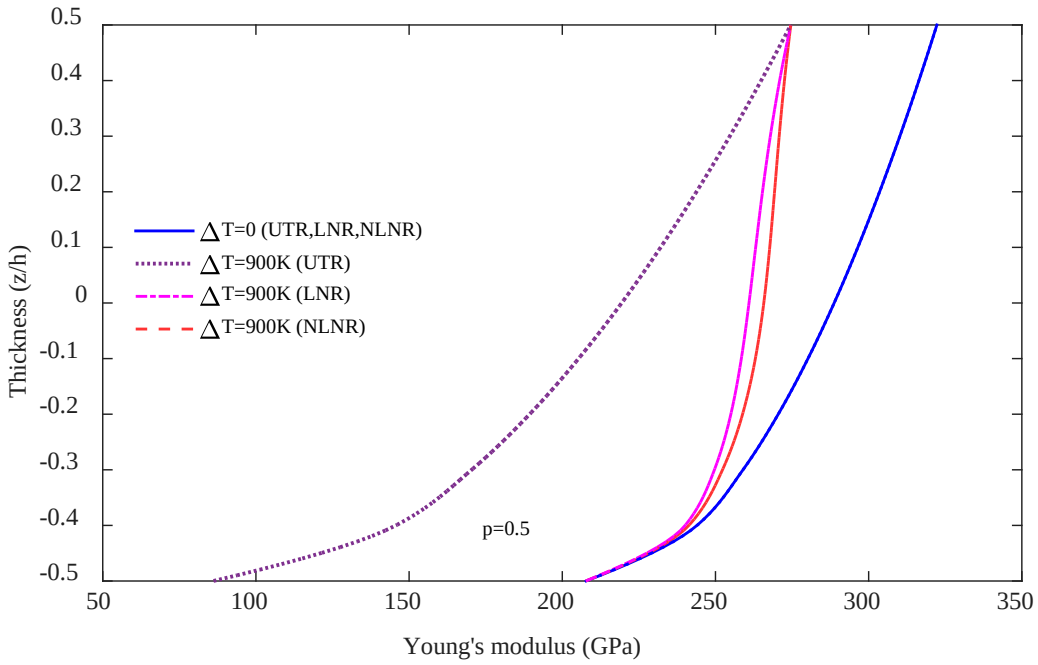

b) Young's modulus of Si_3N_4/SUS304 beams.

Fig. 5: Temperature distributions and Young's modulus of Si_3N_4/SUS304 beams through the thickness with $\Delta T = 0$ and 900K.

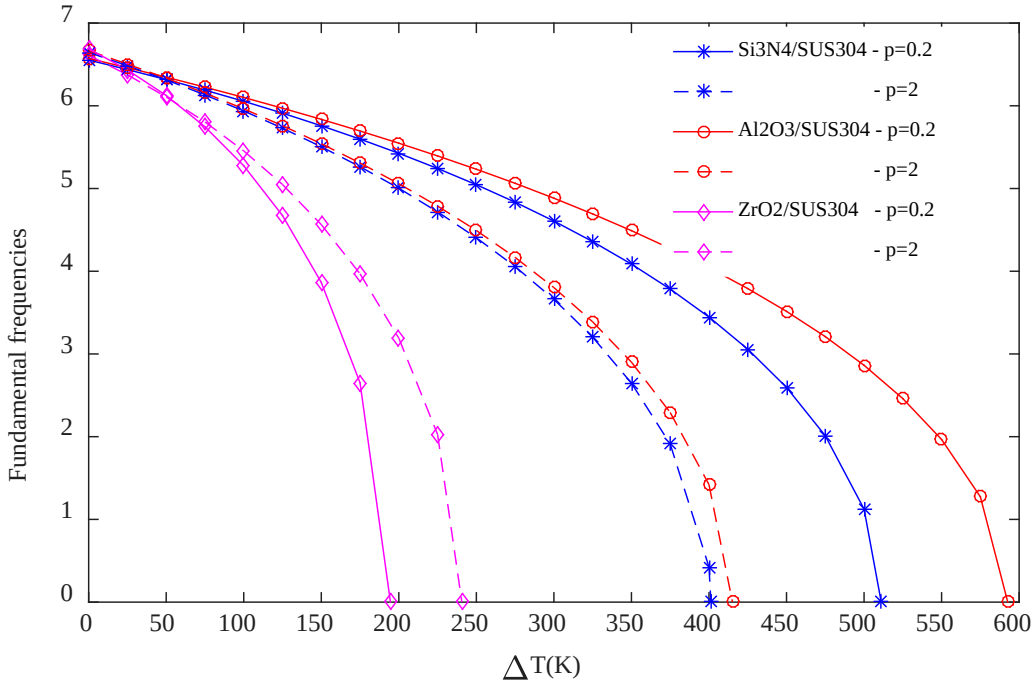

Fig. 6: The first temperature – frequency curves of $C-C$ FG beams $(a/h=20)$.

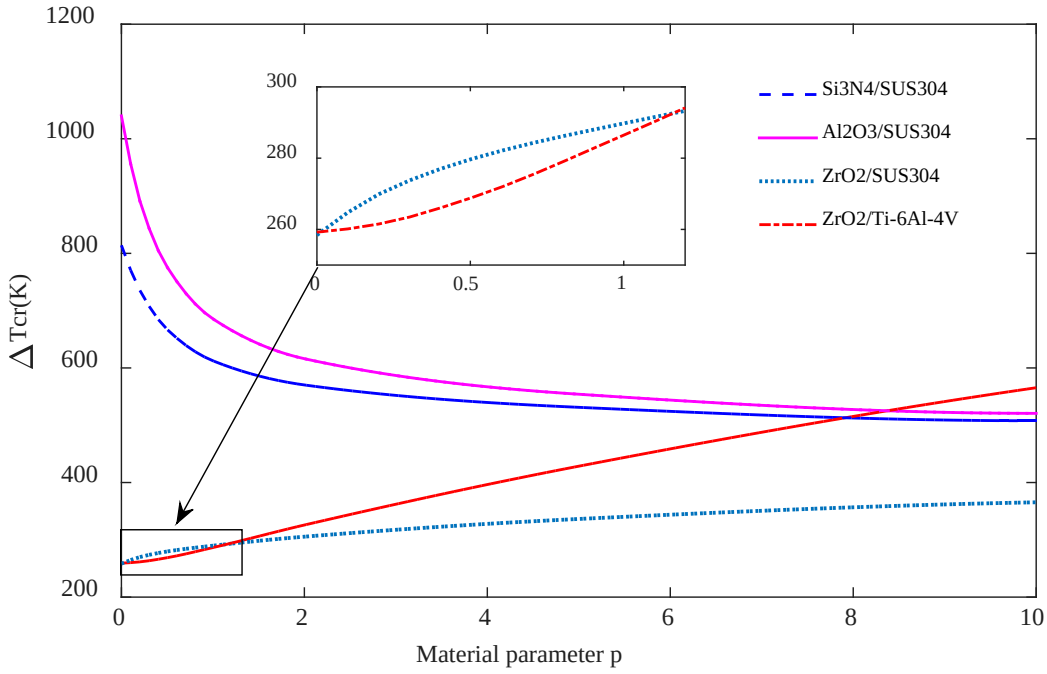

Fig. 7: The effect of material parameters on the critical temperatures of various FG beams under LNR $\left(C-P, a/h=20\right)$.

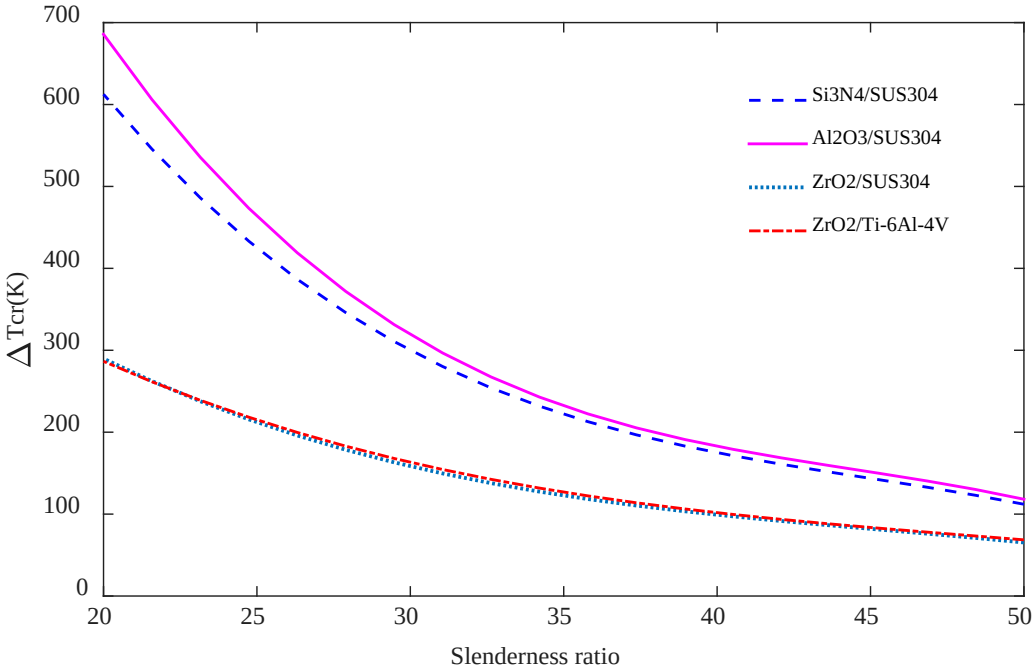

Fig. 8: The effect of slenderness ratios on the critical temperatures of $C-P$ Si_3N_4/SUS304 beam under UTR, LNR and NLNR $(p=0.5)$.

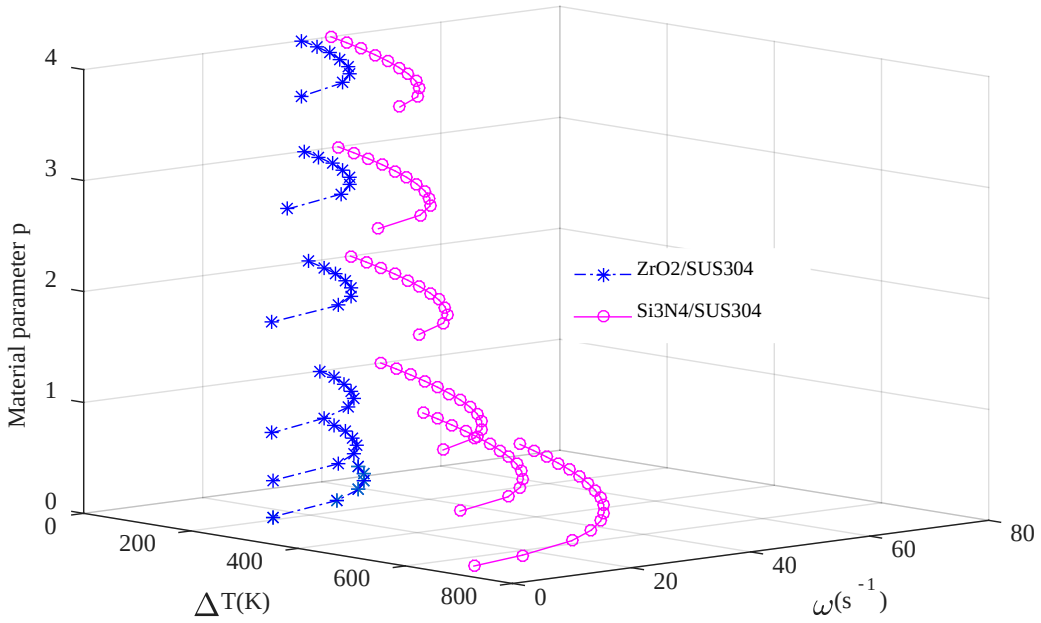

Fig. 9: Frequency – temperature – material parameter interaction curves of Si_3N_4/SUS304 and ZrO_2/SUS304 beams under NLNR.